Investigation of gated cone-beam CT to reduce respiratory motion blurring

Russell E. Kincaid, Jr. and Ellen D. Yorke
Department of Medical Physics, Memorial Sloan-Kettering Cancer Center, New York, New York 10065

Karyn A. Goodman, Andreas Rimner, and Abraham J. Wu
Department of Radiation Oncology, Memorial Sloan-Kettering Cancer Center, New York, New York 10065

Gig S. Mageras[a)]
Department of Medical Physics, Memorial Sloan-Kettering Cancer Center, New York, New York 10065

(Received 31 August 2012; revised 28 December 2012; accepted for publication 27 February 2013; published 20 March 2013)

Purpose: Methods of reducing respiratory motion blurring in cone-beam CT (CBCT) have been limited to lung where soft tissue contrast is large. Respiration-correlated cone-beam CT uses slow continuous gantry rotation but image quality is limited by uneven projection spacing. This study investigates the efficacy of a novel gated CBCT technique.
Methods: In gated CBCT, the linac is programmed such that gantry rotation and kV image acquisition occur within a gate around end expiration and are triggered by an external respiratory monitor. Standard CBCT and gated CBCT scans are performed in 22 patients (11 thoracic, 11 abdominal) and a respiration-correlated CT (RCCT) scan, acquired on a standard CT scanner, from the same day serves as a criterion standard. Image quality is compared by calculating contrast-to-noise ratios (CNR) for tumors in lung, gastroesophageal junction (GEJ) tissue, and pancreas tissue, relative to surrounding background tissue. Congruence between the object in the CBCT images and that in the RCCT is measured by calculating the optimized normalized cross-correlation (NCC) following CBCT-to-RCCT rigid registrations.
Results: Gated CBCT results in reduced motion artifacts relative to standard CBCT, with better visualization of tumors in lung, and of abdominal organs including GEJ, pancreas, and organs at risk. CNR of lung tumors is larger in gated CBCT in 6 of 11 cases relative to standard CBCT. A paired two-tailed t-test of lung patient mean CNR shows no statistical significance ($p = 0.133$). In 4 of 5 cases where CNR is not increased, lung tumor motion observed in RCCT is small (range 1.3–5.2 mm). CNR is increased and becomes statistically significant for 6 out of 7 lung patients with > 5 mm tumor motion ($p = 0.044$). CNR is larger in gated CBCT in 5 of 7 GEJ cases and 3 of 4 pancreas cases ($p = 0.082$ and 0.192). Gated CBCT yields improvement with lower NCC relative to standard CBCT in 10 of 11, 7 of 7, and 3 of 4 patients for lung, GEJ, and pancreas images, respectively ($p = 0.0014$, 0.0030, 0.165).
Conclusions: Gated CBCT reduces image blurring caused by respiratory motion. The gated gantry rotation yields uniformly and closely spaced projections resulting in improved reconstructed image quality. The technique is shown to be applicable to abdominal sites, where image contrast of soft tissues is low. [http://dx.doi.org/10.1118/1.4795336]

Key words: image guided radiation therapy, cone-beam CT, respiratory motion, motion management

I. INTRODUCTION

Modern linear accelerators use onboard cone-beam CT (CBCT) for visualizing tumors and organs at risk (OAR), and to correct patient position, just prior to radiation treatment.[1] Current clinical CBCT scan acquisition time is approximately 1 min for a 360° scan. Since the typical patient breathing period is 10–25 times shorter, respiratory motion during a free-breathing scan is unavoidable. Image quality in CBCT is adversely affected by respiratory motion. Respiratory motion blurs the tumor and nearby organs in the images which makes visualization of organ boundaries difficult. Motion of high contrast objects and interfaces causes streak artifacts in the reconstructed images which also reduce image quality. Therefore, motion mitigation strategies are needed during imaging. Furthermore, when treatment localization is affected by respiratory motion, and strategies are applied to manage the motion for treatment, the same strategies should be applied for imaging.[2,3]

Respiration-correlated CBCT (RC-CBCT), also termed 4D-CBCT, on a linac, using slow continuous gantry rotation to produce a series of images over the breathing cycle, has been studied by several investigators.[4–6] These references discuss degradation of imaging quality in the images by view aliasing streak artifacts caused by uneven projection spacing. For this reason, RC-CBCT has been limited to lung where soft tissue contrast is large.[7,8]

Alternative acquisition methods have been used to reduce motion in CBCT of the abdomen. One method is breath-hold (BH) at end expiration (EE), accomplished by breaking the

acquisition into several breath-holds. This approach requires patient cooperation and compliance. In one study, 38% of the patients were not eligible for the active breathing control (ABC) treatment and imaging protocol.[9] Also, anatomical positions can be different between BH and free breathing,[10] so BH CBCT is normally used in conjunction with BH treatment. The other method used in CBCT of the abdomen is abdominal compression, but recent data in the literature show the amount of motion reduction that is achieved at the tumor site is modest on average.[11,12]

Prior studies at our institution investigated different methods of gating a megavoltage (MV) CBCT system to reduce motion artifacts. Sillanpaa *et al.*[13] demonstrated the feasibility of synchronizing gated operation of a linac and MV-CBCT acquisition to verify tumor position for gated lung treatment. Chang *et al.*[14] investigated two methods of respiratory gated MV CBCT, using gated image acquisition and slow continuous gantry rotation, the other with both gated image acquisition and gated rotation. The use of gated rotation avoided nonuniform angular spacing of projection images and thus eliminated the view aliasing streak artifacts when reconstructed with a filtered backprojection algorithm. However, the linac was not designed for gated gantry rotation, thus gantry movement resulted in excessive vibration and mechanical stress. A subsequent patient study by Chang *et al.*[15] used a prototype computer-controlled system to operate the linac, which reduced the vibration during gated rotation but did not eliminate it.

This study investigates a gated CBCT technique in which both gantry rotation and acquisition of kV image projections occur within a respiratory gate. This technique is now possible using a new type of computer-controlled linac (Varian TrueBeam™) which allows programmed gantry motion. The precise control of gantry motion yields uniformly angular-spaced CBCT projection images without gaps. We investigate the ability of gated CBCT to reduce motion blurring in phantom studies and patient studies in both lung and abdominal sites.

II. METHODS

II.A. Gated CBCT overview

Gated CBCT scans are performed on a computer-controlled linac (TrueBeam v1.5, Varian Medical Systems, Palo Alto, CA), which has capabilities for synchronizing motions of all mechanical axes with MV dose delivery and kV image acquisition, either with or without respiratory gating. In a gated CBCT scan, gantry rotation and kV image acquisition occur only within a gate generated from an external respiratory monitoring system (Real-time Position Management System, RPM). The monitoring system consists of a block with four infrared reflective markers, placed on the patient's abdomen and monitored by a stereoscopic camera, and is sensitive to six degrees-of-freedom motion (three translations, three rotations). For gated CBCT, the gate interval is specified in terms of the phase of the respiratory signal.

In the current TrueBeam software, gated CBCT is possible only in a research mode of operation and programmed by means of a script file. Gated rotation of the gantry is enabled only when the MV beam is on, which is programmed as an arc over 360°. In order to minimize patient exposure to MV irradiation, the total beam-on time over the arc is set to 10 monitor units, the jaws are closed to the minimum allowed field size of 1×1 cm^2, and the multileaf collimator is closed such that the position of leaf abutment does not coincide with the jaw-defined opening. The resultant dose from the 6 MV beam, confirmed with ion chamber measurement, is less than 0.025 cGy at the isocenter. Imaging parameters for gated CBCT are similar to those for the nongated CBCT, i.e., 125 kVp, 80 mA, 20 ms, 11 images/s half-fan acquisition (i.e., detector laterally offset 16 cm to obtain a 46 cm reconstructed diameter), 360° rotation. During the gated CBCT scan and at the start of each gate, the gantry accelerates under computer control to reach its target speed of approximately 1 rpm. At the end of each gate the gantry decelerates, reverses direction, and repositions at its location at the time of gate's end. The result yields narrowly spaced projection images without gaps between consecutive gates, although there is sometimes overlap of images at gantry angles at the abutment between gates. Because the gantry starts from a stationary position at the start of each gate, the average gantry speed with gated CBCT is lower and the number of projections is greater than with standard nongated CBCT.

In gated CBCT, the gate is adjusted to minimize the scan time while limiting motion within the gate to less than 30% of the peak to peak actual tumor or surrogate (ungated) motion extent as measured in the respiration-correlated CT (RCCT) scan obtained at treatment simulation. Increasing the gate width shortens the scan time, partly because of the increased duty cycle, and partly because fewer breath cycles are needed, thereby reducing the number of gantry deceleration/acceleration cycles. This increases average rotation speed and results in fewer redundant images at the abutment between gates, and hence less patient imaging dose (discussed further below).

Gated CBCT projections are preprocessed using custom programs written in MATLAB (MathWorks, Inc., Natick, MA) to reorder images by gantry angle, average any redundant images occurring at the same angle, and correct any errors in the x-ray source intensity measurement. The intensity measurement, from a sensor at the x-ray source, is used to normalize the intensity of each projection for all CBCT scans. This is to compensate for variations in x-ray intensity for each projection. We note that at the start of any scan, and particularly at the start of each gate in gated CBCT, the x-ray intensity can be lower by 10% or more. A set of standard CBCT calibration files obtained for the same imaging parameters as the gated CBCT is used to calibrate and correct for attenuation by the bow-tie filter (using an in-air normalization image), Hounsfield units (HU), x-ray spectrum, and scatter. All projection sets are reconstructed using a research version of the Feldkamp-Davis-Kress (FDK) filtered backprojection algorithm[16] (Varian iTools version 1.0.32.0), which includes the same preprocessing, reconstruction,

and postprocessing procedures as the standard clinical software.

II.B. Motion phantom study

We evaluate efficacy and performance of gated CBCT with a respiratory motion phantom[17] (Quasar, Modus Medical Devices, Inc., London, ON, Canada). This phantom consists of a torso shaped section of acrylic with interchangeable cylindrical motion inserts. It moves a platform (representing the chest wall) in the anterior-posterior (AP) direction and synchronously moves the insert in the superior-inferior (SI) direction to simulate patient breathing. The phantom can be programmed to follow a patient's respiratory trace or for adjustable sinusoidal oscillation. The motor driven acrylic insert contains embedded higher density objects. In this study, we consider 10 and 20 mm diameter spheres, and a 30 mm cube. The RPM block is placed on the platform to provide the optical signal for gated operation.

Increasing the gate width shortens the scan time and reduces patient dose but increases the residual motion within the gate. To test and quantify the effects of increasing the gate width, we perform test scans of the respiratory motion phantom with 25%, 35%, and 45% gate widths.

In the first set of measurements, the Quasar phantom is programmed for simple sinusoidal motion, with 3.2 cm peak-to-trough excursion of the cylindrical insert. Three gated CBCT scans are performed, using 25%, 35%, and 45% gates, centered at EE. The gate is widened symmetrically about the 50% (EE) phase, corresponding to the insert being at the most superior position, to isolate the effects of gate width on total number of projection images acquired and scan time.

In the second set of measurements, the Quasar phantom is programmed to follow a patient respiratory trace resulting in 1.4 cm mean excursion of the insert. Four CBCT scans are performed, all 360° scans with 125 kVp, as follows:

1. Clinical "free-breathing" CBCT (standard CBCT), where the gantry rotates continuously at approximately 6°/s while kV projection images are acquired at the maximum rate (11 fps), resulting in 656 projection images, resulting in 1478 mAs.
2. RC-CBCT, where the gantry rotates continuously and slowly at ∼1°/s while kV projection images are acquired only within a respiratory gate for 35% duty cycle around EE. This is meant to provide the approximate equivalent of one bin of sorted RC-CBCT projections resulting from application of the RC-CBCT technique.[4–6] This experimental scan was done only with the phantom, in research mode, using a custom script file. Using the patient trace chosen for this experiment, this scan resulted in 901 projection images (1442 mAs), but the exact number of projections can vary with breathing pattern, which therefore affects the total mAs for the scan.
3. Gated CBCT, with 35% gate centered at EE. Using the patient trace, this scan resulted in 924 projection images (1478 mAs), but the exact number of projections can vary, which therefore affects the total mAs for the scan.
4. Clinical CBCT of static phantom, with cylinder insert fixed at EE to serve as a criterion standard. The scan parameters are the same as scan (#1).

Phantom image quality and the effect of motion blurring is evaluated by comparing contrast-to-noise ratios[4,5] (CNR) of the 20 mm spherical object relative to the surrounding background, μ_o and μ_b are mean pixel intensities inside the spherical and background volumes, respectively, and σ_o is the standard deviation of the intensities inside the spherical volume

$$\mathrm{CNR} = (\mu_o - \mu_b)/\sigma_o. \tag{1}$$

Analysis is performed using a treatment planning system developed at this institution. We wish to compute CNR based on the ground truth spherical volume. The 20 mm spherical object is delineated in the stationary phantom scan and a 5 mm 3D annulus of the surrounding background is constructed around the object. The stationary scan is rigidly registered to each of the three motion phantom scans by matching in a rectangular volume of interest (VOI) containing the spherical object using a normalized cross-correlation cost function[18] (NCC) where $g1$ and $g2$ are pixel intensities, and μ_1 and μ_2 are mean pixel intensities, within the VOI of n voxels on the two images, respectively,

$$\mathrm{NCC} = -\sum_{i=1}^{n}\left[(g1_i - \mu_1) * (g2_i - \mu_2)\right] \Bigg/ \left[\sqrt{\sum_{i=1}^{n}(g1_i - \mu_1)^2} * \sqrt{\sum_{i=1}^{n}(g2_i - \mu_2)^2}\right]. \tag{2}$$

The automated rigid registration optimization uses downhill simplex to minimize the NCC. The delineated sphere and annulus contours are transferred to the other scans using the rigid registrations. CNR is measured for each of the three motion phantom scans. A comparatively larger CNR indicates better agreement of the study image with the spherical volume defined on the stationary phantom (criterion standard) image. Phantom image quality and the effect of motion blurring are evaluated by comparing contrast-to-noise ratios. Congruence between the object in the three motion phantom images and that in the static CBCT is measured by calculating the NCC at the completion of each rigid registration. Axial localization accuracy is evaluated in sagittal images by comparing mean voxel intensity profiles through the 20 mm diameter sphere.

II.C. Patient study

We evaluated the performance of gated CBCT in IRB approved patient studies. Eligible patients were those receiving radiation treatment of a malignancy in lung, gastroesophageal junction (GEJ), or pancreas that exhibited at least 5 mm motion in a RCCT scan obtained at treatment simulation (described below).

Patients received a RCCT scan (eight-slice Lightspeed, GE Medical Systems, Waukesha, WI), typically 2–3 weeks before

the treatment day research scans, as part of their treatment simulation. This RCCT was also used to predict the optimal patient-specific gate position and width for the gated CBCT scan. The RCCT is obtained from a cine scan which is acquired while recording the patient's respiration (Varian RPM). Acquisition time per couch position is set to the patient's respiration period plus 1 s, with gantry rotation period of 0.5 s. The time interval between consecutive images is the greater of either 1/20 of the couch position acquisition time or 0.25 s. Slice width is 0.25 cm. The slices are sorted into ten phase bins (GE Advantage 4D) that comprise the RCCT image set.

Patient simulation day RCCT images and breathing traces were screened for image artifacts due to irregular breathing, namely, discontinuity artifact in images at end inspiration (EI), and irregular period or amplitude in their breathing trace. During the accrual of the patient data presented in this work, no patients were excluded because of this requirement. Three GEJ patient data sets were not included in this analysis, for the following reasons. One patient had fiducial streaking throughout all CBCT slices in the GEJ making it impossible to visually align the region for analysis. A second patient had an esophageal stent that extended through the GEJ into the stomach making the images inappropriate for similar analysis and comparison to the others. The third patient did not understand the instructions and breathed extremely erratically which made the CBCT and RCCT images unusable. GEJ patients allergic to oral barium contrast or pancreas patients allergic to IV iodine contrast were excluded from the study. Patient data analyzed in the study included 11 in lung, seven GEJ, and four pancreas. The 22 patients included 10 females and 12 males. The mean age was 65.9 years (standard deviation 12.8, range 43–95).

In order to determine an appropriate gate width and location, a tumor motion trajectory vs RPM phase is determined from the simulation RCCT as follows. The 50% phase bin image is chosen as the nominal EE image and the other nine images are each registered rigidly to it, without rotation, using an automatic rigid registration algorithm that minimizes a normalized cross-correlation function of voxel intensities [Eq. (2)] within a VOI that includes either the tumor or implanted markers near the tumor. The 3D registration displacements are plotted, as a function of phase bin, in the AP/SI plane, and in the left-right (LR)/SI plane, to represent the 3D tumor respiratory motion trajectory. In addition, abdominal displacement (RPM block height) recorded during the x-ray on intervals of the scan is plotted as a function of phase. Both plots are considered for the choice of gate: the former to minimize internal target motion within the gate, and the latter to confirm that abdominal motion correlates with the phase assignments. A phase gate is chosen of approximately 35% (25%–50%, mean 35.6%) duty cycle around EE.

Patients enrolled in the protocol underwent research scans on one day in the first week of treatment, consisting of a gated CBCT in nonclinical mode, a standard CBCT in clinical mode prior to treatment, and a standard CBCT in clinical mode after treatment. In addition, they received a RCCT scan on a multislice CT scanner (GE Lightspeed), either before or after the treatment session. Patients were advised to relax and breathe regularly. The research scans per patient resulted in about 20 cGy to the tumor and surrounding tissues. Because the gated CBCT was carried out in a nonclinical mode of operation, a medical physicist experienced in gated CBCT operation was always present to guide the radiation therapist through the procedure. Following completion of the gated CBCT, the linac was returned to the clinical mode of operation prior to acquiring the standard CBCT and administering treatment. The IRB approval of the protocol included the acquisition of gated CBCT in the nonclinical mode under the conditions described here.

For the purposes of the analysis in this paper, comparison of gated CBCT and standard CBCT was different for each disease site: (1) In lung, the gated CBCT was compared to the standard CBCT prior to treatment. (2) In GEJ, patients received 200 cc oral contrast containing 2% barium sulfate suspension prior to the gated CBCT scan. The gated CBCT was compared to the standard CBCT prior to treatment, such that the oral contrast was visible in both CBCT images. (3) In pancreas, the gated CBCT was compared to the standard CBCT after treatment. We note parenthetically that pancreatic patients received intravenous (IV) contrast prior to the pretreatment standard CBCT scan. Therefore, in order to minimize the influence of residual IV contrast, the pretreatment standard CBCT was not used in the analysis of pancreatic cases. In all three disease sites, the RCCT image acquired on the same day served as a criterion standard in the comparison.

We visually assess the differences in image quality, between standard CBCT and gated CBCT, by comparing tumor and organ visibility and boundary sharpness, the presence of streak artifacts in transaxial images, and motion blurring in coronal and sagittal images. In addition, we quantitatively assess the improvement in image quality and accuracy by comparing standard CBCT and gated CBCT images to the RCCT image acquired on the same day. In order to minimize irregular breathing artifacts, the cine scan is amplitude binned to create the RCCT images. For some patients, there are gaps (missing data) at some couch positions caused by variable breathing amplitudes, and in these cases we use motion predicted RCCT images as described in Hertanto *et al.*[19] Image quality is evaluated using the CNR [Eq. (1)] of the gross tumor volume (GTV), or a portion of the diseased organ, relative to the surrounding background tissue. The GTV and background volume for determining CNR are delineated on the same-day RCCT and transferred to the CBCT images, in the following fashion.

In the lung tumor cases, the GTV delineated by the physician on the planning CT is used as a guide to delineate the GTV on the RCCT image at EE, and a 5 mm 3D annulus containing parenchymal lung is constructed around the object. Rigid registration of the RCCT image to each of the CBCT images is performed within a VOI containing the GTV and by minimizing NCC [Eq. (2)] as previously described. The automatic registration is visually inspected and if needed, a manual adjustment is made to visually align the tissue borders in the region of interest. The GTV and annulus contours are transferred from the RCCT to the CBCT images. The process of registration and contour transfer is repeated 3–4 times,

on different days, to determine the variability of the CNR measurement.

For computation of CNR in the GEJ cases, the GTV, esophagus, and stomach delineated by the physician on the planning CT are used as a guide to delineate, on the RCCT image at EE, a portion of the GEJ excluding implanted fiducial markers, and a 5 mm background region of lower density neighboring tissue. The portion chosen is along the anterior border of the GEJ with the two contoured regions inside and outside the GEJ tissue plane. Care is taken to avoid the lumen of the esophagus and the gas within it, which can affect the CNR measurement. The RCCT image is rigidly registered to each of the CBCT images in a VOI enclosing the GEJ and contoured regions, but excluding fiducial markers, and the contours are transferred as described for the lung cases.

For computation of CNR in the pancreatic cases, a portion of the tail of the pancreas is delineated on the RCCT image at EE, along with a 5 mm background region of lower density neighboring adipose tissue. The RCCT image is rigidly registered to each of the CBCT images in a VOI enclosing the pancreas tail and contoured regions and the contours are transferred as described for the lung cases. For all patients, all contours were delineated by a physicist and reviewed by a physician.

In all cases, similarity in object size and shape between the CBCT and RCCT is measured by calculating the optimized NCC after alignment of the object using CBCT-to-RCCT rigid registration. The rigid registration serves to remove any object displacement caused by setup error and patient movement that may have occurred between the RCCT, gated CBCT, and standard CBCT scans.

III. RESULTS

III.A. Motion phantom study

Table I summarizes the measurements with the motion phantom programmed for sinusoidal motion. As the gate is increased from 25% to 45% of the motion cycle, there is a reduction in scan time, total projections, and x-ray exposure. For a gate of 35% (45%), relative to a 25% gate, actual scan time is reduced by 38% (53%), compared to the 29% (44%) reduction predicted by the increase in gate width. Similarly, the total number of projections for the 35% (45%) gate width is reduced 13% (17%) relative to that for the 25% gate width. These further reductions, caused by fewer breath cycles per scan, are due to fewer repeat images at the abutment between consecutive gates and to the larger average gantry speed within the longer gates. We note that because a sinusoidal motion trace was used, a smaller fraction of the time was spent near EE than is more typically the case for patient breathing. A motion trace more typical of patients would have resulted in a larger number of images per gate, and reduced the relative effects described above.

TABLE I. Scan parameters and statistics for scans of Quasar motion phantom using sinusoidal motion with 3.8 s period.

Width of gate [% of cycle]	Projections/ scan	Scan duration [min:s]	Cycles/ scan	Projections/ cycle	Scan exposure [mAs]
25	990	5:58	94.2	10.5	1584
35	857	3:42	58.4	14.7	1371
45	823	2:47	43.9	18.7	1317

Figure 1 compares transaxial and sagittal CBCT images acquired using various CBCT acquisition modes when the phantom motion is programmed to follow a patient breathing trace (Fig. 1). A scan of the stationary phantom serves as a criterion standard (top left and bottom left panels). The gated CBCT image (middle left and second bottom panels) shows less streak artifacts in the transaxial image than RC-CBCT due to more uniformly spaced projections, and less motion blurring than standard CBCT in the sagittal image due to the smaller amount of motion within the gate. The RC-CBCT image (top right and third bottom panels) shows pronounced streak artifacts in the transaxial image and more noise in the sagittal image than any other mode due to unevenly spaced projections. Motion blurring in the sagittal RC-CBCT image is similar to gated CBCT and less than standard CBCT. The standard CBCT (middle right and bottom right panels) shows slightly more motion induced streak artifacts in the transaxial image than gated CBCT, and more motion blurring in the sagittal image than any other mode.

Figure 2 compares profiles of mean voxel intensity, averaged over six pixels in the AP direction, along the direction of motion (SI) through the 20 mm diameter sphere in the sagittal images in Fig. 1. The three profile intensities were shifted to minimize their root mean squared (RMS) deviation from the static phantom profile. The root mean squared deviation, in CT numbers, is 31.7, 90.7, and 56.7 for gated CBCT, standard CBCT, and RC-CBCT, respectively. The shallower falloff near the sphere boundary in the gated CBCT and RC-CBCT profiles, relative to the stationary phantom image and reflected in the nonzero RMS deviation, is owing to the residual motion within the gate. The profile for the RC-CBCT images shows the effect of noise caused by reconstruction artifacts from unevenly spaced projections resulting in a larger RMS deviation than for the gated CBCT. The standard CBCT profile shows more shallow falloff and larger RMS deviation than the gated CBCT.

CNR in the motion phantom images, for a VOI containing the 20 mm diameter sphere and surrounding background annulus, is calculated using the criterion-standard contours from the static phantom images. CNR for gated CBCT, RC-CBCT, and standard CBCT is 3.44, 2.11, and 2.68, respectively. CNR for gated CBCT is larger than for RC-CBCT (ratio 1.63) and for standard CBCT (1.28). NCC for gated CBCT, RC-CBCT, and standard CBCT is −0.944, −0.858, and −0.870, respectively (where −1 corresponds to perfect correlation). NCC for gated CBCT is improved over RC-CBCT (ratio 1.10) and over standard CBCT (1.09).

III.B. Patient studies in lung

Figure 3 compares standard and gated CBCT images of a free-breathing patient with a tumor in the right lung that

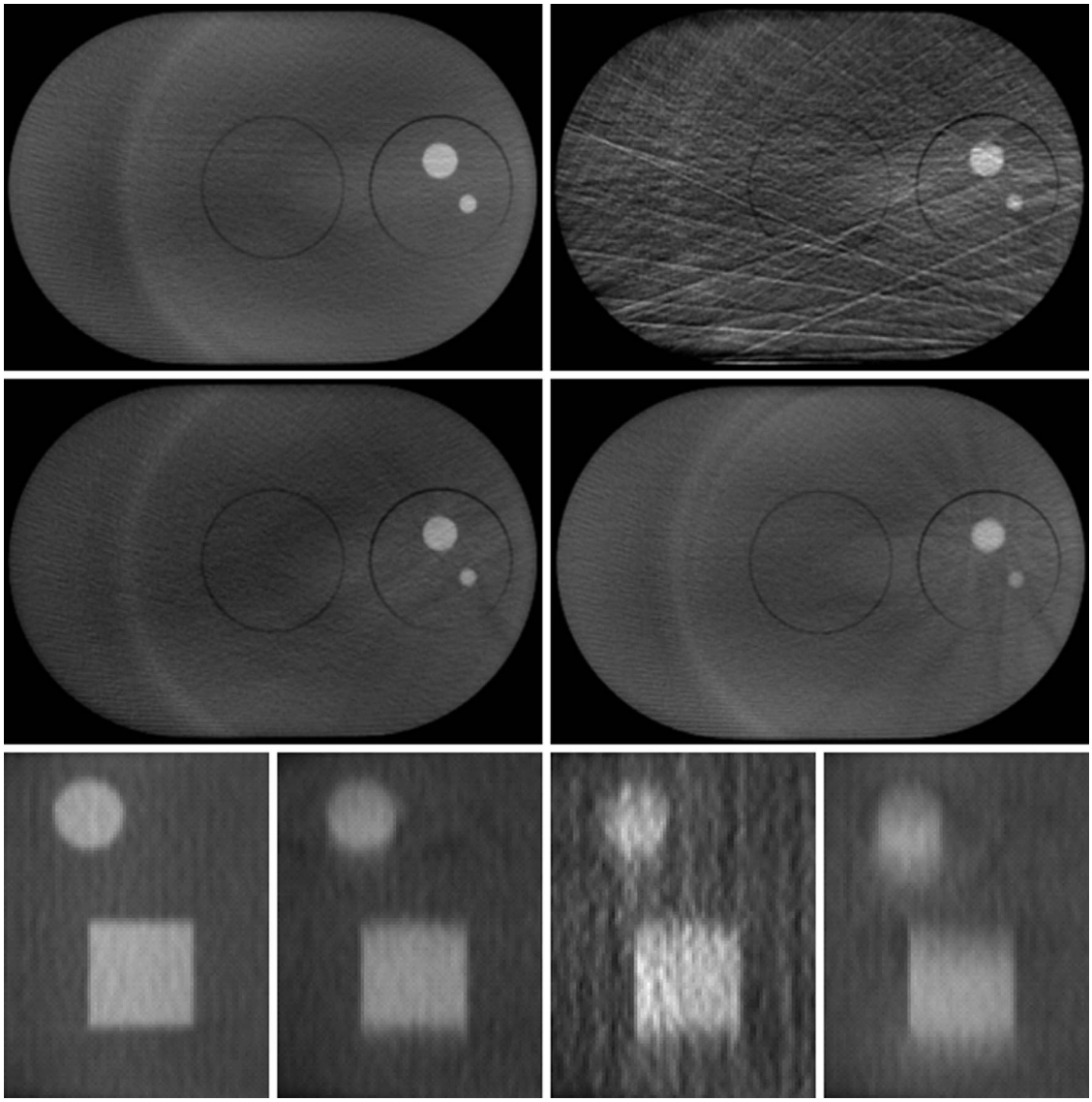

FIG. 1. CBCT images of the motion phantom using various acquisition modes. Transaxial images (top and middle rows) include the entire phantom with higher density 10 and 20 mm diameter spheres. (Top left) Standard CBCT scan of stationary phantom; (middle left) gated CBCT with gate centered at one extreme of the motion ("EE"); (top right) RC-CBCT at EE; (middle right) standard CBCT. Sagittal images (bottom row) are 2× magnification of a region with the 20 mm diameter sphere and a 30 mm cube. Motion in three rightmost panels is along the axial (S-I) direction (vertical in image). (Left to right) Standard CBCT scan of stationary phantom, gated CBCT with gate centered at one extreme of the motion ("EE"), RC-CBCT at EE, standard CBCT.

undergoes respiratory motion. The RPM phase gate used for this patient (patient 4) is 25%–65%. The number of projections acquired is 1244 and the scan duration is 4:53 [min:s]. The image planes intersect at the tumor. The same window/level settings are used for both images. A visual comparison of gated CBCT images to standard CBCT images of this patient shows features including the tumor and the diaphragm appear sharper and clearer in the gated CBCT. Standard CBCT shows more motion induced streak artifact in the transaxial image and more motion blurring in the coronal image than gated CBCT (Fig. 3).

Figure 4 compares tumor CNR between standard and gated CBCT in 11 patients with lung tumors. Gated CBCT shows increase of CNR in 6 out of 11 patients. A paired two-tailed *t*-test of lung patient mean CNR shows no statistical significance ($p = 0.133$). For 4 of the 5 patients where there is no CNR improvement tumor motion extent is small (mean 3.2 mm, range 1.3–5.2 mm), as measured in the RCCT, and so gating brings little or no benefit. Gated CBCT shows increase of CNR in 6 out of 7 patients with >5 mm tumor motion extent (patients 1–6 and 10). A paired two-tailed *t*-test of lung patient mean CNR for these 7 patients shows there is statistical significance ($p = 0.044$).

Figure 5 compares, for standard and gated CBCT, the normalized cross-correlation following rigid registration of the CBCT to the RCCT image. Gated CBCT yields lower NCC in 10 of 11 patients. A paired two-tailed *t*-test of lung patient mean NCC shows there is statistical significance ($p = 0.0014$). This indicates higher congruence with the criterion-standard RCCT at EE for gated CBCT than standard CBCT. Gated CBCT yields lower NCC in 7 of 7 patients with > 5 mm tumor motion extent (patients 1–6 and 10). A paired

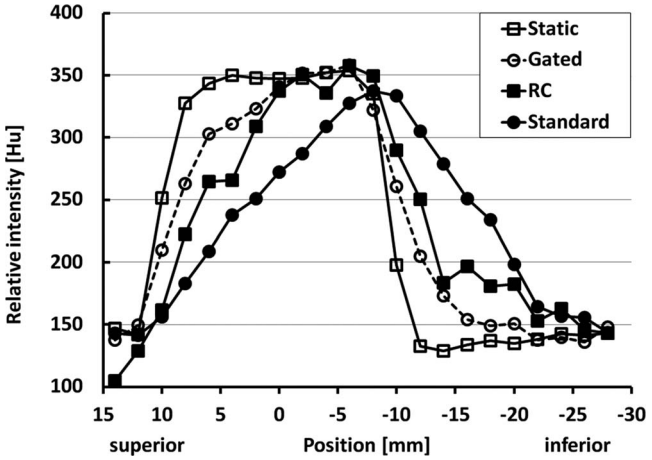

FIG. 2. Mean voxel intensity profiles in longitudinal direction across 20 mm diameter sphere in motion phantom. "RC" denotes respiration correlated CBCT. Mean intensity is calculated from six voxels in direction perpendicular to motion (i.e., along the horizontal in the bottom row of Fig. 1). Each profile is normalized by minimizing the RMS deviation from the static phantom profile.

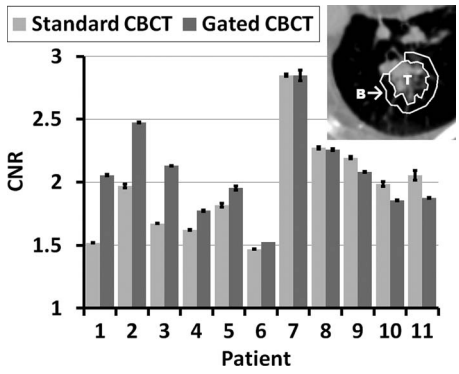

FIG. 4. CNR for 11 patients with tumor in lung, in order of decreasing difference in CNR between gated and standard CBCT. Inset shows example tumor and background regions for calculation of CNR.

two-tailed *t*-test of lung patient mean NCC for these 7 patients shows there is statistical significance ($p = 0.00037$).

III.C. Patient studies in gastroesophageal junction

Figure 6 compares standard and gated CBCT images of a free-breathing patient with a GEJ tumor that undergoes respiratory motion. The RPM phase gate used for this patient (patient 1) is 35%–65%. The number of projections acquired is 1072 and the scan duration is 5:56 [min:s]. The image planes intersect at the GEJ. The patient was given oral barium contrast before the start of the gated CBCT scan. The standard CBCT scan started 3:52 [min:s] after the end of the gated scan. The same window/level settings are used for both images. A visual comparison of gated CBCT images to standard CBCT images of this patient show finer features and sharper organ boundaries in the gated CBCT. Motion artifacts in standard CBCT severely limit visibility of the GEJ, whereas the GEJ is clearly visible in gated CBCT. Standard CBCT shows more motion induced streak artifact in the transaxial image and more motion blurring in the coronal image than gated CBCT (Fig. 6).

Figure 7 (left panel) compares GEJ-to-background CNR between standard and gated CBCT in seven patients with malignancy in GEJ. Gated CBCT shows larger CNR relative to standard CBCT in five out of seven patients. Cases of negative CNR are those in which the mean intensity of the

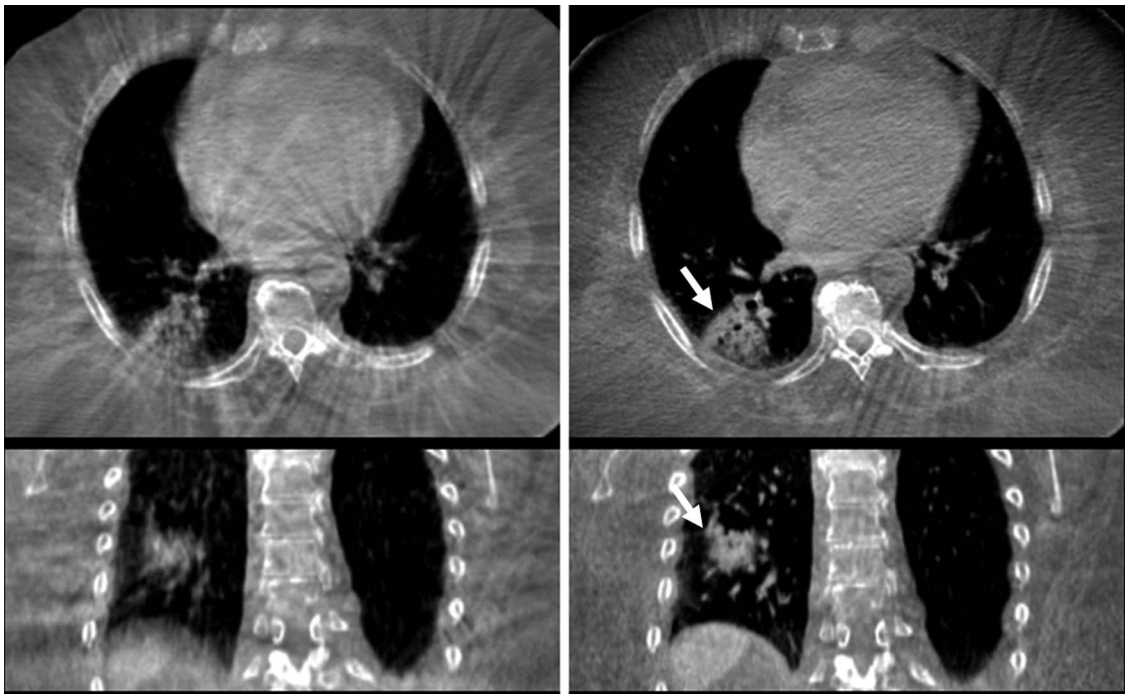

FIG. 3. (Top and bottom) Transaxial and coronal CBCT images of free-breathing patient with tumor in right lung. Image planes intersect in the tumor. Left column is standard CBCT, right is gated CBCT. Arrows indicate lung tumor in the gated CBCT.

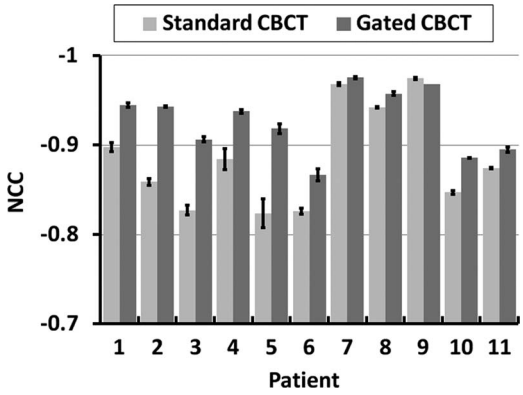

FIG. 5. Zero suppressed plot of NCC for 11 patients with tumor in lung.

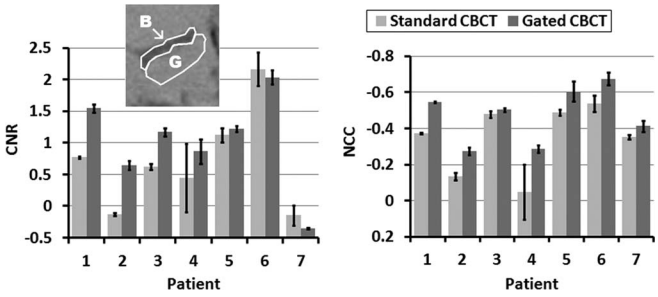

FIG. 7. (Left panel) Gastroesophageal junction CNR for seven patients, in order of decreasing difference in CNR between gated and standard CBCT. Inset shows example regions used for calculating CNR (G - GE junction, B - background). (Right panel) NCC for same patients.

background is greater than that of the object. A paired two-tailed t-test of CNR in these patients shows no statistical significance ($p = 0.082$).

Figure 7 (right panel) compares, for standard and gated CBCT, the normalized cross-correlation following rigid registration of the CBCT to the RCCT image at EE. Gated CBCT yields lower NCC than standard CBCT in seven of seven patients. A paired two-tailed t-test of NCC in these patients shows there is statistical significance ($p = 0.0030$). This indicates higher congruence with the criterion-standard RCCT at EE for gated CBCT than standard CBCT.

III.D. Patient studies in pancreas

Figure 8 compares standard and gated CBCT images of a free-breathing patient treated for pancreatic cancer. The RPM phase gate used for this patient (patient 1) is 35%–70%. The number of projections acquired is 889 and the scan duration is 3:54 [min:s]. The image planes intersect in the pancreas, inferior to the fiducial. The patient was given intravenous iodine contrast after the gated CBCT scan, at the start of the standard CBCT scan before treatment. For the purposes of this analysis, the gated CBCT is compared to the post-treatment standard CBCT (approximately 15 min after the intravenous contrast was administered), in order to minimize differences in the two scans caused by the contrast. The residual iodine causes the standard CBCT to appear brighter than the gated CBCT. The same window/level settings are used for both images. A visual comparison of gated CBCT images to standard CBCT images of this patient shows finer features and sharper organ boundaries in the gated CBCT. Motion artifacts in standard CBCT severely limit visibility of the pancreas and nearby organs, whereas the pancreas is clearly visible in

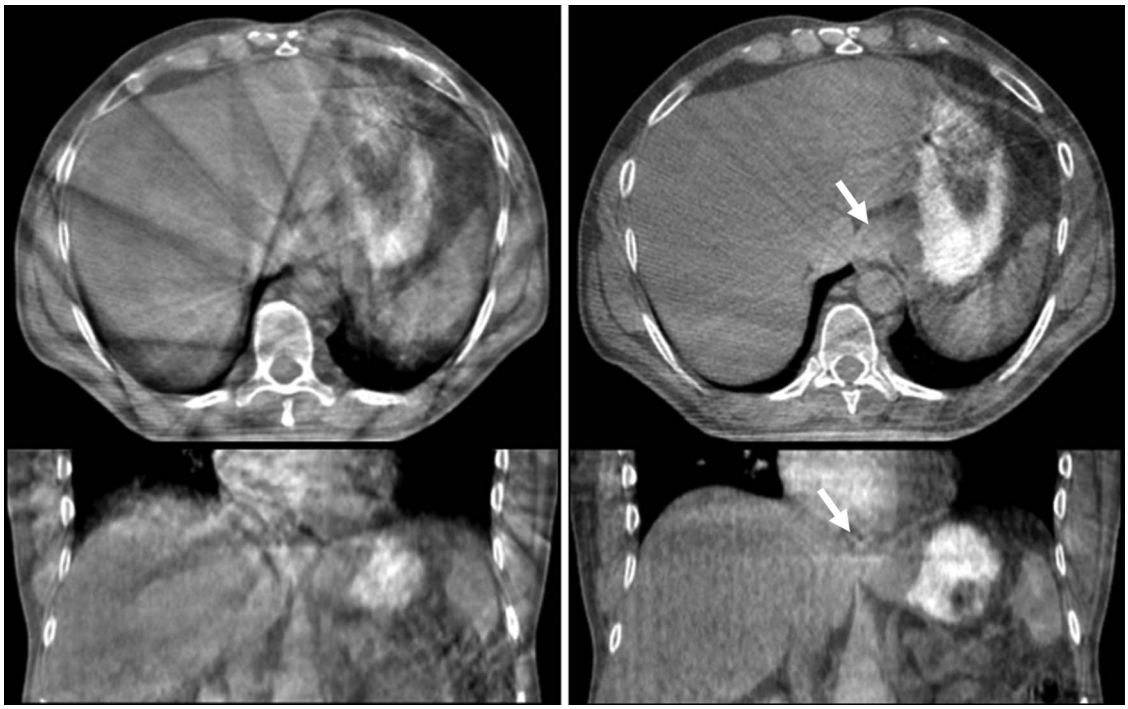

FIG. 6. (Top and bottom) Transaxial and coronal CBCT images of free-breathing patient with tumor in GE Junction. Image planes intersect in the GEJ. Left column is standard CBCT, right is gated CBCT. Arrows indicate GEJ in the gated CBCT.

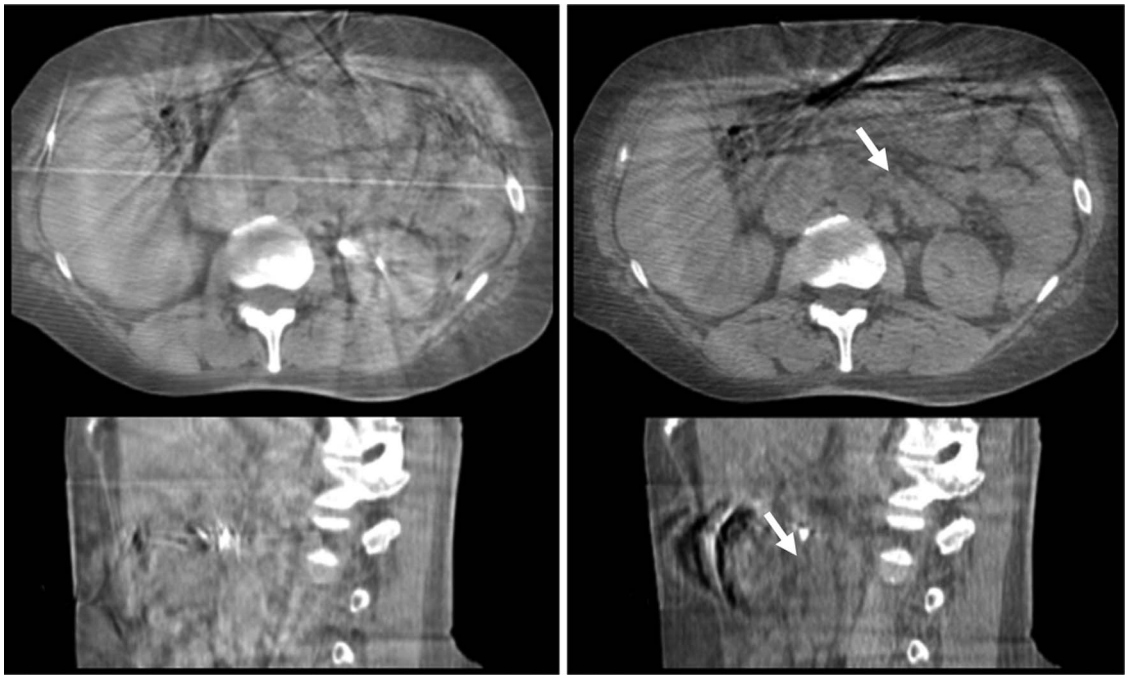

FIG. 8. Transaxial and sagittal CBCT images of a free-breathing patient treated for pancreatic cancer. Image planes intersect in the pancreas, inferior to the fiducial. Left column is standard CBCT, right is gated CBCT. Arrows indicate pancreas in the gated CBCT.

the transaxial and sagittal gated CBCT images. In addition, there is a clear reduction in the blurring of the fiducial. Standard CBCT shows more motion induced streak artifact in the transaxial image and more motion blurring in the sagittal image than gated CBCT (Fig. 8).

Figure 9 (left panel) compares pancreas CNR between standard and gated CBCT in four patients with malignancy in pancreas. Gated CBCT shows larger CNR relative to standard CBCT in three out of four patients. A paired two-tailed *t*-test of CNR in these patients shows no statistical significance ($p = 0.192$). We note that for the one patient where gated CBCT does not bring CNR improvement, disease has caused noticeable atrophy to the tail region of the pancreas, which was used for this study. For the other three patients, where there is CNR improvement, a paired two-tailed *t*-test of mean CNR improves statistically ($p = 0.096$).

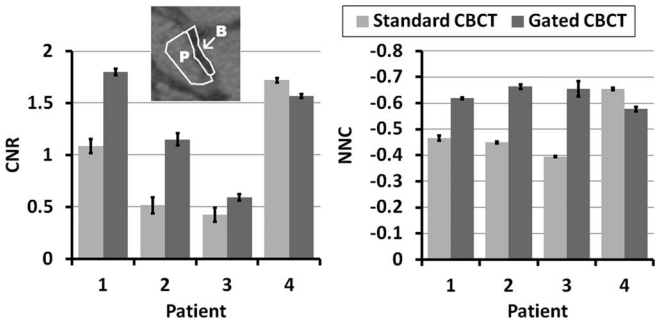

FIG. 9. (Left panel) CNR for four patients treated for pancreatic cancer, in order of decreasing difference in CNR between gated and standard CBCT. Inset shows example regions used for calculating CNR (P - pancreas tail, B - background). (Right panel) NCC for same patients.

Figure 9 (right panel) compares, for standard and gated CBCT, the normalized cross-correlation following rigid registration of the CBCT to the RCCT image at EE. Gated CBCT yields lower NCC than standard CBCT in three of four patients, indicating higher congruence with the criterion-standard RCCT at EE than for standard CBCT. A paired two-tailed *t*-test of NCC in these patients shows no statistical significance ($p = 0.165$). When we exclude the one patient with atrophy to the tail region of the pancreas, NCC for the other three patients becomes statistically significant ($p = 0.020$).

IV. DISCUSSION AND CONCLUSIONS

Our studies in phantom and patient data indicate that gated CBCT reduces image blurring and streaking artifacts caused by respiratory motion. By using recent computer controlled linac technology to gate gantry rotation, projection images within a RPM-defined gate interval that are uniformly and closely spaced can be acquired. Gated CBCT images of a motion phantom show a reduction of streak artifacts and noise, relative to RC-CBCT images, that are acquired with uneven projection spacing. In patient and motion phantom images, gated CBCT shows less motion induced streak artifact in transaxial images, and less motion blurring in coronal and sagittal images, than standard CBCT.

The technique is applicable to respiratory sites such as lung and abdomen. Gated CBCT images in lung show sharper definition of tumor and diaphragm than standard CBCT. In abdomen, where soft tissue visibility in standard CBCT is more difficult due to motion-induced streaking artifacts, gated CBCT shows finer features and sharper organ boundaries than standard CBCT. Gated CBCT in abdomen provides improved

ability to visualize and localize tumor-bearing organs and nearby organs at risk. Our findings indicate improved CNR, and congruence of lung tumors and abdominal organs with those in RCCT as measured by NCC, in most patients in which motion of the target organ exceeds 5 mm.

In gated CBCT, the goal is to limit residual target motion within the gate to approximately 30% or less of the total motion extent. To achieve this, our study uses simulation day RCCT images to predict the optimal patient-specific gate position and width. A possible limitation of this technique is the use of an external marker on the abdomen which is dependent on correlation with the internal anatomy. Feng *et al.*[20] reported that pancreatic tumor border position did not correlate with abdominal wall or diaphragm position. However, Wang *et al.*[21] found that variations in tidal volume and diaphragmatic excursion correlated strongly with superior-inferior GEJ displacement. Although our studies showed improved CNR and NCC in three out of four pancreas patients, they require confirmation with a larger number of patients.

Changes in time lag between internal and external motion signals can affect the performance of gating based on an external signal. Published studies have reported on internal-external time lag and changes in time lag between treatment sessions.[22–24] We account for time lag by selecting a RPM phase-based gate that is centered on tumor motion about the end expiration position in the simulation RCCT. The procedure followed in this study therefore assumed constancy in time lag between simulation and the first week of treatment, in which the gated CBCT scan occurs. Change in time lag, between simulation and treatment, or between treatment sessions, is a potential problem because the gate might no longer be centered on the extremum of internal motion. Within-gate verification images during treatment provide an important check of gating accuracy.[25] Along those lines one could acquire and analyze a short fluoroscopic sequence at the treatment machine just prior to the gated scan, determine the time lag between internal motion, by visualizing the tumor, a fiducial, or the diaphragm, and motion of the external marker and compare it with the time lag measured in the prior RCCT. In the event of change, the gate position for the CBCT can be adjusted accordingly. Furthermore, this updated gate position could then be used in the case of gated treatment. Such an approach would require software that quickly analyses the fluoro images prior to the scan.

Another limitation of the method is longer scan duration, mean ~5 min (range 3–8 min), depending on gate width and breathing period. The actual scan duration depends on the patient breathing behavior during the scan.

Because gated CBCT acquires projections over only a part of the respiration cycle, it potentially results in less patient dose than RC-CBCT. It yields a 3D image at one motion state, thus providing no motion information, in contrast to RC-CBCT which provides motion information but whose applicability has been limited to tumors in lung. Studies in lung, by Sonke *et al.*[7] and independently by Bissonnette *et al.*,[8] found that interfraction baseline variations, i.e., variations in the respiration-averaged position of lung tumors, were larger than amplitude variations. These studies suggest that in most cases it may be sufficient to acquire a CBCT of improved image quality, gated at a single phase interval in the breathing cycle, and correct for tumor position at this phase interval, instead of measuring the full tumor trajectory using RC-CBCT. For small changes in amplitude, for example, tumor position at end expiration will correlate closely with the respiration-averaged position. Changes in breathing amplitude could instead be monitored using a short fluoroscopic sequence and comparing tumor or diaphragm excursion to that observed in a prior (planning day) RCCT. If the amplitude has changed such that the respiration-averaged tumor position may be different, then a correction to account for this could be calculated using the amplitude difference in the fluoroscopic sequence and comparing it to the amplitude difference in the RCCT. The resultant scale factor could be applied to calculate the respiration-averaged tumor position using the tumor position observed in the gated CBCT at end expiration. Furthermore, if lung anatomical changes that may affect tumor motion extent are observed in the gated CBCT, such as tumor shrinkage or resolution of atelectasis, a RC-CBCT could be acquired to re-establish the tumor-diaphragm motion relationship. As well, better images allow better assessment of tumor shrinkage (or growth) during the course of treatment, providing information for adaptive treatment changes.

A potentially important application of gated CBCT is the improved soft tissue visualization for assessing target coverage and OAR sparing, particularly in abdomen. This would be possible because one could more accurately register the gated CBCT with the EE scan from simulation and verify that anatomical changes during the course of treatment have not shifted an OAR into the high dose region. Gated CBCT thus provides information not available through implanted fiducial markers, which are generally limited to a few locations in or near the target.

Gated CBCT is also potentially applicable to gated treatment, although in this study we did not compare tumor or surrogate positions with images acquired during treatment delivery. For gated treatment, a consistent motion state is desirable for all imaging and treatment, thus the same gating system and gating conditions are preferable.[2,3] In this study, gated CBCT was investigated under free-breathing conditions without coaching. In the case of gated treatment with coaching, the simulation RCCT and gated CBCT would also be carried out with coaching.

ACKNOWLEDGMENTS

This work was supported in part by Award No. R01-CA126993 from the National Cancer Institute. The content is solely the responsibility of the authors and does not necessarily represent the official views of the National Cancer Institute or the National Institutes of Health. Memorial Sloan-Kettering has a research agreement with Varian Medical Systems. The authors thank Michelle Svatos and Stefan Scheib for assistance with the research mode of the Varian TrueBeam, Timo Berkus for assistance with the Varian research cone-beam tomographic reconstruction software, Assen Kirov for assistance with gated CBCT scan dosimetry,

and Joseph McNamara for assistance with and helpful discussions concerning the Quasar motion phantom.

[a]Author to whom correspondence should be addressed. Electronic mail: magerasg@mskcc.org; Telephone: 646-888-5615.

[1]D. A. Jaffray, J. H. Siewerdsen, J. W. Wong, and A. A. Martinez, "Flat-panel cone-beam computed tomography for image-guided radiation therapy," Int. J. Radiat. Oncol., Biol., Phys. **53**, 1337–1349 (2002).

[2]S. B. Jiang, "Technical aspects of image-guided respiration-gated radiation therapy," Med. Dosim. **31**, 141–151 (2006).

[3]S. B. Jiang, J. Wolfgang, and G. S. Mageras, "Quality assurance challenges for motion-adaptive radiation therapy: Gating, breath holding, and four-dimensional computed tomography," Int. J. Radiat. Oncol., Biol., Phys. **71**, S103–S107 (2008).

[4]J.-J. Sonke, L. Zijp, P. Remeijer, and M. van Herk, "Respiratory correlated cone beam CT," Med. Phys. **32**, 1176–1186 (2005).

[5]T. Li, L. Xing, P. Munro, C. McGuinness, M. Chao, Y. Yang, B. Loo, and A. Koong, "Four-dimensional cone-beam computed tomography using an on-board imager," Med. Phys. **33**, 3825–3833 (2006).

[6]J. Lu, T. M. Guerrero, P. Munro, A. Jeung, P.-C. M. Chi, P. Balter, X. R. Zhu, R. Mohan, and T. Pan, "Four-dimensional cone beam CT with adaptive gantry rotation and adaptive data sampling," Med. Phys. **34**, 3520–3529 (2007).

[7]J. J. Sonke, J. Lebesque, and M. van Herk, "Variability of four-dimensional computed tomography patient models," Int. J. Radiat. Oncol., Biol., Phys. **70**, 590–598 (2008).

[8]J.-P. Bissonnette, K. N. Franks, T. G. Purdie, D. J. Moseley, J.-J. Sonke, D. A. Jaffray, L. A. Dawson, and A. Bezjak, "Quantifying interfraction and intrafraction tumor motion in lung stereotactic body radiotherapy using respiration-correlated cone beam computed tomography," Int. J. Radiat. Oncol., Biol., Phys. **75**, 688–695 (2009).

[9]M. A. Hawkins, K. K. Brock, C. Eccles, D. Moseley, D. Jaffray, and L. A. Dawson, "Assessment of residual error in liver position using kV cone-beam computed tomography for liver cancer high-precision radiation therapy," Int. J. Radiat. Oncol., Biol., Phys. **66**, 610–619 (2006).

[10]P. J. Keall, G. S. Mageras, J. M. Balter, R. S. Emery, K. M. Forster, S. B. Jiang, J. M. Kapatoes, D. A. Low, M. J. Murphy, B. R. Murray, C. R. Ramsey, M. B. Van Herk, S. S. Vedam, J. W. Wong, and E. Yorke, "The management of respiratory motion in radiation oncology report of AAPM Task Group 76," Med. Phys. **33**, 3874–3900 (2006).

[11]C. L. Eccles, R. Patel, A. K. Simeonov, G. Lockwood, M. Haider, and L. A. Dawson, "Comparison of liver tumor motion with and without abdominal compression using cine-magnetic resonance imaging," Int. J. Radiat. Oncol., Biol., Phys. **79**, 602–608 (2011).

[12]K. Han, P. Cheung, P. S. Basran, I. Poon, L. Yeung, and F. Lochray, "A comparison of two immobilization systems for stereotactic body radiation therapy of lung tumors," Radiother. Oncol. **95**, 103–108 (2010).

[13]J. Sillanpaa, J. Chang, G. Mageras, H. Riem, E. Ford, D. Todor, C. C. Ling, and H. Amols, "Developments in megavoltage cone beam CT with an amorphous silicon EPID: Reduction of exposure and synchronization with respiratory gating," Med. Phys. **32**, 819–829 (2005).

[14]J. Chang, J. Sillanpaa, C. C. Ling, E. Seppi, E. Yorke, G. Mageras, and H. Amols, "Integrating respiratory gating into a megavoltage cone-beam CT system," Med. Phys. **33**, 2354–2361 (2006).

[15]J. Chang, G. S. Mageras, E. Yorke, F. De Arruda, J. Sillanpaa, K. E. Rosenzweig, A. Hertanto, H. Pham, E. Seppi, A. Pevsner, C. C. Ling, and H. Amols, "Observation of interfractional variations in lung tumor position using respiratory gated and ungated megavoltage cone-beam computed tomography," Int. J. Radiat. Oncol., Biol., Phys. **67**, 1548–1558 (2007).

[16]L. A. Feldkamp, L. C. Davis, and J. W. Kress, "Practical cone-beam algorithm," J. Opt. Soc. Am. A. **1**, 612–619 (1984).

[17]C. W. Hurkmans, M. van Lieshout, D. Schuring, M. J. T. van Heumen, J. P. Cuijpers, F. J. Lagerwaard, J. Widder, U. A. van der Heide, and S. Senan, "Quality assurance of 4D-CT scan techniques in multicenter phase III trial of surgery versus stereotactic radiotherapy (radiosurgery or surgery for operable early stage (stage 1A) non-small-cell lung cancer [ROSEL] study)," Int. J. Radiat. Oncol., Biol., Phys. **80**, 918–927 (2011).

[18]R. C. Gonzales and R. E. Woods, *Digital Image Processing* (Addison-Wesley, Reading, MA, 1992), p. 584.

[19]A. Hertanto, Q. Zhang, Y. C. Hu, O. Dzyubak, A. Rimner, and G. S. Mageras, "Reduction of irregular breathing artifacts in respiration-correlated CT images using a respiratory motion model," Med. Phys. **39**, 3070–3079 (2012).

[20]M. Feng, J. M. Balter, D. Normolle, S. Adusumilli, Y. Cao, T. L. Chenevert, and E. Ben-Josef, "Characterization of pancreatic tumor motion using cine MRI: Surrogates for tumor position should be used with caution," Int. J. Radiat. Oncol., Biol., Phys. **74**, 884–891 (2009).

[21]J. Wang, S. H. Lin, L. Dong, P. Balter, R. Mohan, R. Komaki, J. D. Cox, and G. Starkschall, "Quantifying the interfractional displacement of the gastroesophageal junction during radiation therapy for esophageal cancer," Int. J. Radiat. Oncol., Biol., Phys. **83**, e273–e280 (2012).

[22]D. Ionascu, S. B. Jiang, S. Nishioka, H. Shirato, and R. I. Berbeco, "Internal-external correlation investigations of respiratory induced motion of lung tumors," Med. Phys. **34**, 3893–3903 (2007).

[23]S. S. Korreman, T. Juhler-Nottrup, and A. L. Boyer, "Respiratory gated beam delivery cannot facilitate margin reduction, unless combined with respiratory correlated image guidance," Radiother. Oncol. **86**, 61–68 (2008).

[24]K. J. Redmond, D. Y. Song, J. L. Fox, J. Zhou, C. N. Rosenzweig, and E. Ford, "Respiratory motion changes of lung tumors over the course of radiation therapy based on respiration-correlated four-dimensional computed tomography scans," Int. J. Radiat. Oncol., Biol., Phys. **75**, 1605–1612 (2009).

[25]R. E. Wurm, F. Gum, S. Erbel, L. Schlenger, D. Scheffler, D. Agaoglu, R. Schild, B. Gebauer, P. Rogalla, M. Plotkin, K. Ocran, and V. Budach, "Image guided respiratory gated hypofractionated Stereotactic Body Radiation Therapy (H-SBRT) for liver and lung tumors: Initial experience," Acta Oncol. **45**, 881–889 (2006).